Available online at www.sciencedirect.com

ScienceDirect

Proceedings of the Combustion Institute 38 (2021) 2673–2680

Proceedings of the Combustion Institute

www.elsevier.com/locate/proci

In-Situ Adaptive Manifolds: Enabling computationally efficient simulations of complex turbulent reacting flows

Cristian E. Lacey*, Alex G. Novoselov, Michael E. Mueller

Department of Mechanical and Aerospace Engineering, Princeton University, Princeton, NJ 08544, USA

Received 7 November 2019; accepted 8 June 2020
Available online 25 August 2020

Abstract

Reduced-order manifold approaches to turbulent combustion modeling traditionally involve precomputation of manifold solutions and pretabulation of the thermochemical database versus a small number of manifold variables. However, additional manifold variables are required as the complexity of turbulent combustion processes increases through consideration of, for example, multi-modal, non-adiabatic, or non-isobaric combustion, or combustion featuring multiple and/or inhomogeneous inlets. This increase in the number of manifold variables comes with an increase in the computational cost of precomputing a greater number of manifold solutions, most of which are never actually utilized in a CFD calculation. The memory required to store the pretabulated high-dimensional thermochemical database also increases, practically limiting the complexity of manifold-based combustion models. In this work, a new In-Situ Adaptive Manifolds (ISAM) approach is developed that overcomes this limitation by combining 'on-the-fly' calculation of manifold solutions with In-Situ Adaptive Tabulation (ISAT), enabling the use of more complex manifold-based turbulent combustion models. The performance of ISAM is evaluated via LES of turbulent nonpremixed jet flames with both hydrogen and hydrocarbon fuels. A performance assessment indicates that the computational overhead associated with ISAM compared to pretabulation ranges from negligible up to a factor of two, with most of this overhead associated with convolution of the thermochemical state against a presumed subfilter PDF. In addition, the memory requirements of ISAM are more than two orders of magnitude less than conventional tabulation. These results demonstrate the potential for ISAM to accommodate significantly more complex manifold-based combustion models.
© 2020 The Combustion Institute. Published by Elsevier Inc. All rights reserved.

Keywords: Manifold-based modeling; In-Situ Adaptive Tabulation (ISAT); Turbulent nonpremixed combustion; Large Eddy Simulation (LES)

1. Introduction

In practical systems, turbulent combustion is characterized by very small scales that cannot be fully resolved using Direct Numerical Simulation (DNS). Therefore, these small-scale turbulent combustion processes must be modeled in the context of Large Eddy Simulation (LES) or Reynolds-Averaged Navier–Stokes (RANS). However, practical fuels require hundreds or even thousands of chemical species to fully describe their combustion chemistry, making the unresolved

* Corresponding author.
E-mail address: clacey@princeton.edu (C.E. Lacey).

https://doi.org/10.1016/j.proci.2020.06.207
1540-7489 © 2020 The Combustion Institute. Published by Elsevier Inc. All rights reserved.

state-space extremely high-dimensional. This fact severely limits brute-force modeling approaches that solve an additional transport equation for each relevant chemical species (e.g., the Transported PDF approach [1] or the Linear Eddy Model [2]).

Instead, the dimensionality of the unresolved combustion processes can be reduced using a reduced-order manifold. This approach characterizes the underlying combustion process with far fewer manifold variables, and a manifold mapping is required to project the high-dimensional space of the species mass fractions and an energy variable onto the low-dimensional space of the manifold variables. The manifold is typically constructed by making *a priori* assumptions about the nature of the combustion processes, usually that they occur in the limit of a single asymptotic mode of combustion, either premixed combustion, nonpremixed combustion, or homogeneous autoignition. The manifold mapping is typically expressed in terms of a differential equation for the thermochemical state in terms of the manifold variables, hereafter referred to as the manifold equation. In an LES or RANS calculation, transport equations are evolved or algebraic relationships are evaluated for the manifold variables, and the thermochemical state is determined from solutions to the manifold equations. As commonly implemented, solutions to the manifold equations are precomputed and pretabulated against the manifold variables.

The dimensionality of the manifold increases with model complexity as additional physics are considered including multi-modal combustion [3,4], heat losses [5,6], pressure variation [7], or multiple and/or inhomogeneous stream mixing [8–10]. However, this increase in the dimensionality of the manifold poses two challenges to conventional approaches relying on precomputation and pretabulation of the manifold solutions. First, as the dimensionality increases, an increasing number of manifold solutions are computed, whether actually ultimately needed or not during an LES or RANS calculation. Second, the memory requirement for storing the precomputed database becomes insurmountable. Some efforts have focused on using either parallel computing [11,12] or alternative data structures [13,14] to at least partially mitigate the memory requirement issue, but these approaches still rely on precomputation of a large number of potentially unneeded manifold solutions.

Simply stated, as the dimensionality of the manifold increases, not all of the manifold solutions will be required over the course of a simulation, and precomputation of unneeded solutions is wasted effort. In this work, rather than using precomputed and pretabulated manifold solutions, a far more efficient and sensible approach is developed in which manifold calculations are performed 'on-the-fly' and adaptively tabulated using In-Situ Adaptive Tabulation (ISAT) [15]. This approach, termed In-Situ Adaptive Manifolds (ISAM), would enable more complex and general manifold models. This manuscript focuses on nonpremixed combustion, leveraging the steady flamelet model as a vehicle to evaluate the implementation and computational overhead of ISAM in LES with variation in chemical mechanism sizes.

2. Manifold-based modeling for turbulent nonpremixed combustion

2.1. Steady flamelet model

For the case of adiabatic, nonpremixed combustion with two inlets (fuel and oxidizer), the thermochemical state can be expressed in terms of the mixture fraction and the mixture fraction dissipation rate. This formulation involves defining the local mixture fraction Z, which is zero in the oxidizer stream and unity in the fuel stream, as a conserved scalar with unity Lewis number [16]. The governing equations for the species mass fractions in physical space and time can be transformed into mixture fraction space. Assuming unity effective Lewis numbers [17], this transformation results in the steady flamelet equations [18]:

$$0 = \frac{\rho \chi_{ZZ}}{2} \frac{d^2 Y_k}{dZ^2} + \dot{m}_k \,, \tag{1}$$

where ρ is the density, $\dot{m}_k$ is the chemical source term, and χ_{ZZ} is the mixture fraction dissipation rate. A similar equation can be formulated for the temperature. With this model, the thermochemical state $\boldsymbol{\phi}$ is expressed as a function of the mixture fraction and the mixture fraction dissipation rate:

$$\phi(\mathbf{x}, t) = \phi(Z[\mathbf{x}, t], \chi_{ZZ}[\mathbf{x}, t]) \,. \tag{2}$$

Solution of Eq. (1) requires a presumed dependence of the dissipation rate on the mixture fraction, which is based on an analytical solution for the dissipation rate in a counterflow flame [19]:

$$\chi_{ZZ}(Z) = \chi_{\text{ref}} \frac{f(Z)}{f(Z_{\text{ref}})} \,, \tag{3}$$

where

$$f(Z) = \exp\left(-2\left[\text{erfc}^{-1}(2Z)\right]^2\right) . \tag{4}$$

The characteristic reference value for the dissipation rate χ_{ref} is evaluated at the stoichiometric mixture fraction.

2.2. Coupling with LES

In LES, the filtered thermochemical state is required, which can be obtained through convolution of the manifold against a presumed subfilter PDF for the manifold variables, in this case, the mixture fraction:

$$\tilde{\phi}_k = \int \phi_k(Z; \chi_{\text{ref}}) \tilde{P}(Z; \tilde{Z}, Z_v) dZ \,. \tag{5}$$

The density-weighted subfilter PDF of the mixture fraction $\tilde{P}(Z;\tilde{Z},Z_v)$ is presumed to be a beta distribution [20], parameterized by the filtered mixture fraction $\tilde{Z}$ and its corresponding subfilter variance Z_v, which is obtained from its transport equation.

The filtered mixture fraction dissipation rate can be obtained from the gradient of the filtered mixture fraction [21]:

$$\tilde{\chi}_{ZZ} = 2D\widetilde{\frac{\partial Z}{\partial x_j}\frac{\partial Z}{\partial x_j}} \approx 2(\tilde{D}+D_{\text{sfs}})\frac{\partial \tilde{Z}}{\partial x_j}\frac{\partial \tilde{Z}}{\partial x_j}, \tag{6}$$

where D_{sfs} is the subfilter diffusivity. From the presumed dependence of the dissipation rate on the mixture fraction (Eq. (3)), the reference mixture fraction dissipation rate can be obtained through deconvolution, presuming no subfilter variation of the reference dissipation rate:

$$\tilde{\chi}_{ZZ} = \chi_{\text{ref}}\int \frac{f(Z)}{f(Z_{\text{ref}})}\tilde{P}(Z;\tilde{Z},Z_v)dZ. \tag{7}$$

As a result, the filtered thermochemical state can be expressed in terms of either the filtered mixture fraction dissipation rate or the reference mixture fraction dissipation rate:

$$\begin{aligned}\tilde{\phi}(\mathbf{x},t) &= \tilde{\phi}\big(\tilde{Z}[\mathbf{x},t],Z_v[\mathbf{x},t],\tilde{\chi}_{ZZ}[\mathbf{x},t]\big)\\ &= \tilde{\phi}\big(\tilde{Z}[\mathbf{x},t],Z_v[\mathbf{x},t],\chi_{\text{ref}}[\mathbf{x},t]\big).\end{aligned} \tag{8}$$

3. In-Situ Adaptive Manifold (ISAM) approach

Two operations are required to obtain the filtered thermochemical state in Eq. (8): computation of the solutions of the manifold equations (Eq. (1)) and convolution of the manifold solutions against the presumed subfilter PDF of the mixture fraction (Eq. (5)). Different software implementations are possible depending on when these operations occur.

3.1. Conventional approach: precomputation, preconvolution, and pretabulation (PPP)

In the conventional implementation, the solutions to the manifold equations are computed, convoluted against the presumed subfilter PDF, and tabulated before the LES. For the steady flamelet model, the precomputed, preconvoluted, and pretabulated (PPP) database $\mathcal{T}_{\text{PPP}}$ depends on the filtered mixture fraction, subfilter mixture fraction variance, and reference dissipation rate (or filtered dissipation rate):

$$\mathcal{T}_{\text{PPP}} : \widetilde{\phi} = \widetilde{\phi}\big(\widetilde{Z},Z_v,\chi_{\text{ref}}\big). \tag{9}$$

For this relatively simple combustion model, computation and storage of this database is not difficult, requiring up to several minutes of computational time and hundreds of MB of memory, depending on the size of the chemical mechanism considered and the number of thermochemical variables stored in the database. However, as manifold dimensionality increases for more complex models, the computational cost and storage requirements quickly become impractical.

3.2. Convolution-on-the-fly (COTF)

In an effort to reduce the dimensionality of the precomputed table for more complex models with additional manifold coordinates, Perry and Mueller [22] implemented a strategy in which only the manifold solutions were precomputed and pretabulated. Convolution against the presumed subfilter PDF was conducted on-the-fly during the LES, that is, convolution-on-the-fly (COTF). In the case of the steady flamelet model, the dimensionality of the precomputed database $\mathcal{T}_{\text{COTF}}$ is reduced and depends only on the mixture fraction and the reference mixture fraction dissipation rate:

$$\mathcal{T}_{\text{COTF}} : \phi = \phi(Z,\chi_{\text{ref}}). \tag{10}$$

Of course, the trade-off is that one must perform the convolution operation on-the-fly, but Perry and Mueller [22] demonstrated that this could potentially be more computationally efficient than retrieving the filtered thermochemical state from higher-dimensional tables in addition to enabling more complex subfilter PDF models with several (co-)variances that would dramatically increase the dimensionality of a preconvoluted database.

3.3. In-Situ Adaptive Manifolds (ISAM)

Even with COTF, the problem of precomputing and storing unaccessed manifold states still remains. Only a small portion of the manifold space may actually be sampled over the course of an LES, and the time and memory used to compute the potentially large number of unaccessed states of the manifold could be reclaimed by solving the manifold equations as the simulation proceeds. However, unlike with convolution against the presumed subfilter PDF, which is implemented simply as a scalar product, the solution of the manifold equations, even the steady flamelet equations, is computationally non-trivial. Therefore, rather than repeatedly solving the same set of manifold equations on-the-fly as is done in the in-situ flamelet-generated manifolds (IFM) approach by Lodier et al. [23], solutions to the manifold equations must be saved and reused subsequently in the LES. Efficient reuse is accomplished by storing and retrieving manifold solutions using In-Situ Adaptive Tabulation (ISAT) [15].

3.3.1. Overview of ISAT

ISAT relies on a binary tree data structure that is adaptively constructed as the database is queried. Consider a generic input-output $\boldsymbol{y}(\boldsymbol{x})$, where both the inputs and outputs can be vectors. Each leaf of the tree is associated with a particular value of

the input $\boldsymbol{x}^0$ and an "ellipsoid of accuracy" within which a local linear approximation to the output satisfies a user-specified error tolerance (combination of a relative and an absolute tolerance). With each query to the ISAT database with input $\boldsymbol{x}^q$, the binary tree is traversed to locate a nearby $\boldsymbol{x}^0$ and determine whether the query point is located within the corresponding ellipsoid of accuracy. Typically, one of three outcomes is possible:

1. *Retrieval*: If the query point is within the ellipsoid of accuracy, return the local linear approximation to the output:
$$\boldsymbol{y}(\boldsymbol{x}^q) \approx \boldsymbol{y}(\boldsymbol{x}^0) + \boldsymbol{J}^0(\boldsymbol{x}^q - \boldsymbol{x}^0), \tag{11}$$
where $\boldsymbol{J}^0$ is the Jacobian matrix at $\boldsymbol{x}^0$.
2. *Growth*: If the query point is not within the ellipsoid of accuracy, explicitly evaluate the output. If the resulting difference between the explicit evaluation and the local linear approximation is less than the user-specified error tolerance, then expand the ellipsoid of accuracy to include the query point.
3. *Addition*: If the query point is not within the ellipsoid of accuracy, explicitly evaluate the output. If the resulting difference between the direct evaluation and the local linear approximation is greater than the user-specified error tolerance, then add a new leaf corresponding to the query point $\boldsymbol{x}^q$.

3.3.2. ISAT implementation with the steady flamelet model

With the steady flamelet model, the lone input $\boldsymbol{x}$ to the ISAT database is the reference scalar dissipation rate χ_{ref}. The discrete solutions to Eq. (1) for every thermochemical quantity of interest $\phi_j(Z_k; \chi_{\text{ref}})$, where ϕ_j is each thermochemical quantity of interest and Z_k are the discrete points in mixture fraction space, are aggregated as the output $\boldsymbol{y}$. Over the course of the LES, at each grid point at each timestep, the reference dissipation rate is computed and input to ISAT. For each thermochemical quantity of interest, the outputs from ISAT, which are discrete functions of the mixture fraction, are convoluted against the presumed subfilter PDF of the mixture fraction (a beta distribution). The weights are precomputed and pretabulated as in the COTF algorithm [22]. The ultimate output is the filtered thermochemical state which is updated in the LES code. However, only the unfiltered thermochemical state is stored in ISAT.

The current implementation uses a separate ISAT table for each MPI process. The tables are not synced at any point during the simulation, meaning that thermochemical states previously computed by one MPI process and needed by another are inaccessible, requiring some redundant computation. Additionally, domain decomposition across MPI processes is static and uniform in terms of the grid points per MPI process. Ideally, the domain would be decomposed such that approximately a uniform number of manifold solutions are computed on each MPI process for more efficient load balancing. Syncing ISAT tables across MPI processes and introducing dynamic load balancing could therefore both improve ISAM performance in the future, and the present implementation could be viewed as a 'worst-case' implementation in terms of computational overhead.

4. Test configurations

4.1. Computational infrastructure

To test the newly-developed ISAM approach, two canonical turbulent nonpremixed jet flames were simulated using NGA- a structured, finite-difference, low Mach number flow solver [24,25]. For LES, all subfilter transport terms are closed with dynamic Smagorinsky-like models [26], with the exception discussed below. The one-dimensional manifold equations, given by Eq. (1), are solved using the PDRs code [4,27]. To ensure convergence, PDRs starts with the thermodynamic equilibrium profile and evolves the manifold equations in pseudo-time to provide an initial guess for a Newton solver. An analytical Jacobian has also been implemented for the manifold equations, which converges more smoothly than a numerical Jacobian, further ensuring solver convergence.

4.2. Configuration I: hydrogen jet flame

The first configuration is a turbulent nonpremixed hydrogen simple jet flame with a Reynolds number of 10,000 [28–30]. Only pure hydrogen, undiluted by helium, is considered in this work. The flame was simulated in cylindrical coordinates using a stretched grid with $256 \times 144 \times 64$ grid points along the axial, radial, and circumferential directions, respectively. A uniform inlet velocity profile was imposed for the coflow, and the central jet inflow velocity profile was generated from a separate simulation of fully-developed turbulent pipe flow. The chemical mechanism for hydrogen combustion [31] consists of 9 species. The relative and absolute tolerances in ISAT are set to 10^{-3} and 10^{-9}, respectively. For this flame, statistics were computed using a constant Smagorinsky constant of 0.12 and a constant turbulent Schmidt number of 0.7. However, timings are shown with the dynamic models for comparison with the other flame configuration.

4.3. Configuration II: Sandia Flame D

The second configuration is Sandia Flame D, a turbulent piloted partially premixed methane/air jet flame with a Reynolds number of 22,400 [32]. The flame was simulated in cylindrical coordinates using a stretched grid with $256 \times 144 \times 64$ grid

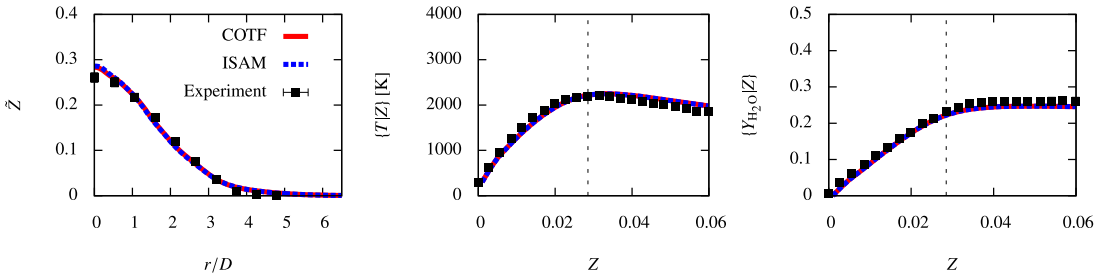

(a) Mixture fraction (b) Temperature (c) Water mass fraction

Fig. 1. Time-averaged statistics at $x/D = 22.5$ for the hydrogen jet flame. The vertical dashed line denotes the stoichiometric mixture fraction $Z_{st} = 0.0285$. The solid line corresponds to COTF, the dashed line to ISAM, and symbols to experimental measurements with estimated uncertainty [28].

points along the axial, radial, and circumferential directions, respectively. Uniform inlet velocity profiles were imposed for the coflow and pilot, and the central jet inflow velocity profile was generated from a separate simulation of fully-developed turbulent pipe flow. The mechanism for methane combustion, GRI-3.0 [33], consists of 35 species with the nitrogen chemistry removed. The relative and absolute tolerances in ISAT are also set to 10^{-3} and 10^{-9}, respectively.

5. Results

The COTF approach is compared to ISAM in order to verify the implementation of the latter, and the two approaches are compared to experimental measurements. The relative computational performance of ISAM is then assessed for both test configurations.

5.1. Results: hydrogen jet flame

Figure 1 compares spatial statistics for the mixture fraction and conditional statistics for the temperature and the water mass fraction. The results with the COTF approach and with ISAM are in good agreement, verifying the ISAM implementation. Both approaches are in good agreement with the experimental measurements for mixture fraction, temperature, and the water mass fraction.

5.2. Results: Sandia Flame D

Figure 2 compares spatial statistics for the mixture fraction and conditional statistics for the temperature and carbon dioxide mass fraction. As for the hydrogen flame, COTF and ISAM are in good agreement, verifying the ISAM implementation for hydrocarbon chemistry. Compared to the experimental measurements, the only major discrepancy is the temperature on the rich side of the flame, but this is consistent with previous studies using the same combustion model, which attributed the error to slight overpredictions of heat release due to the partial premixing of the methane with air [34].

To ensure ISAT tolerances are appropriately selected, a sensitivity analysis is conducted for the ISAT relative error tolerance (the absolute error tolerance is set to an extremely small value). Figure 3 demonstrates that the statistics of Sandia Flame D are insensitive to loosening or tightening of the ISAT relative error tolerance.

5.3. Performance assessment

The performance of ISAM is evaluated by comparing the baseline time elapsed per timestep as each simulation proceeds. The cost per timestep in ISAM fluctuates up to a factor of seven in the worst cases, depending on the number of ISAT retrieves versus additions during a particular timestep. The baseline cost is defined as the "minimum" cost for a timestep in which most ISAT evaluations are simply retrieves. In other words, this cost indicates the overhead of traversing the binary tree constructed by ISAT. This baseline cost becomes increasingly regular as the simulation progresses and the relative number of retrieves versus additions increases. Addition of MPI synchronization of the ISAT tables and dynamic load balancing would reduce the number of manifold solutions required to be computed by each processor and effectively reduce the fluctuations to zero after an initial transient.

Figure 4 demonstrates how the baseline cost of ISAM evolves for the hydrogen jet flame. As one might expect, the cost of the first step is relatively expensive as the ISAT tables are populated from scratch. However, the cost is only a couple of minutes and does not require that the manifold solutions be precomputed, preconvoluted, and pretabulated as in the conventional approach, which typically takes far longer than a few minutes. The cost sharply declines over the first ten timesteps and rapidly reaches a plateau of 6.4 s after approximately 100–1000 timesteps. Remarkably, the additional baseline cost incurred by ISAM is no more than that of convolution-on-the-fly,

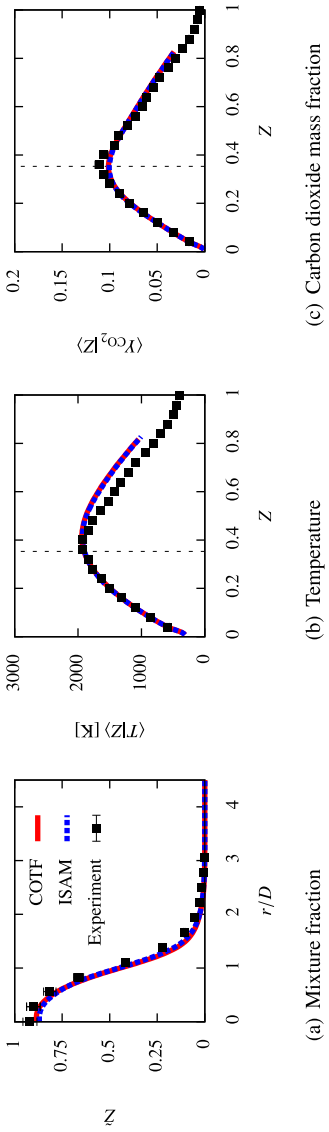

(a) Mixture fraction (b) Temperature (c) Carbon dioxide mass fraction

Fig. 2. Time-averaged statistics at $x/D = 15$ for Sandia Flame D. The vertical dashed line denotes the stoichiometric mixture fraction $Z_{st} = 0.353$. The solid line corresponds to COTF, the dashed line to ISAM, and symbols to experimental measurements with estimated uncertainty [32].

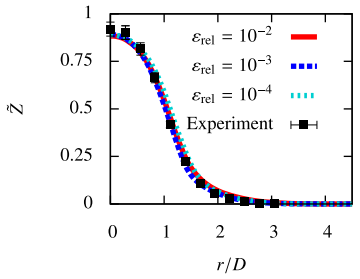

Fig. 3. Time-averaged statistics at $x/D = 15$ for Sandia Flame D. The solid line corresponds to an ISAT relative error tolerance of 10^{-2}, the dashed line to 10^{-3}, the dotted line to 10^{-4}, and symbols to experimental measurements with estimated uncertainty [32].

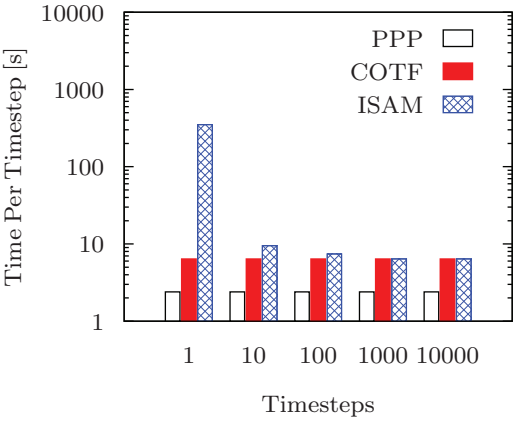

Fig. 4. Baseline computational cost per timestep for the hydrogen jet flame.

implying that traversing the binary tree is nearly negligible in cost for the hydrogen jet flame case.

Figure 5 shows that the cost of COTF is actually less than that of PPP for the Sandia Flame D simulation, also observed by Perry and Mueller [22]. Overhead from convolution can be lower than additional lookup costs from larger tables. Simply stated, as the database grows, memory management with larger tables in PPP can become limiting compared to the relatively cheap floating point operations of convolution against the subfilter PDF in COTF. The figure also illustrates a similar trend in the baseline cost as the hydrogen jet flame, though the initial cost of populating the ISAT tables is greater due to the greater number of species in the methane chemical mechanism. However, the cost of the first timestep is measured in minutes, which is far less than the typical time taken for construction of a conventional PPP database. This cost reduces rapidly, leveling off at 5.7 s, only marginally more than PPP. The number of points per MPI process is the same as for the hydrogen flame, demonstrating that the computational overhead of ISAM

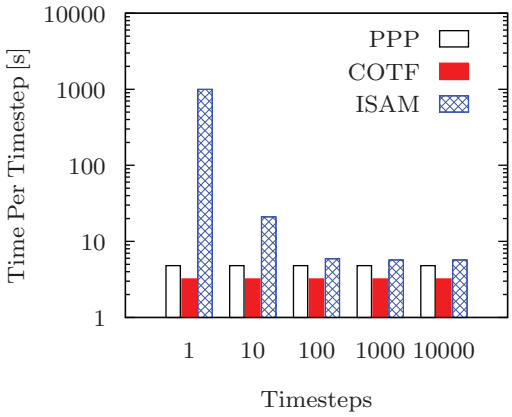

Fig. 5. Baseline computational cost per timestep for Sandia Flame D.

at steady-state does not depend on the size of the chemical mechanism. Therefore, ISAM is feasible even for larger chemical mechanisms.

Additionally, while the computational cost of ISAM and PPP are comparable, the ISAM database size in memory is over 100 times smaller than that of PPP. Though database size is not a limiting factor for the steady flamelet model, this already considerable memory savings will only increase with more complex manifold-based models. While the computational overhead will increase with increased manifold dimensionality and model complexity, ISAT has been used with explicit chemistry exceeding 150 species (see, e.g., Ref. [35]), so even extremely complex manifold-based models should not introduce significant computational overhead. In addition, aside from the first few timesteps in which the manifold solutions are computed to populate the ISAT tables, no significant overhead is incurred for larger chemical mechanisms.

6. Conclusions

A new software implementation that integrates manifold-based modeling approaches and on-the-fly adaptive tabulation has been developed to address problems with existing methods involving pretabulation, which currently limit manifold model complexity. This approach, termed In-Situ Adaptive Manifolds (ISAM), was applied with the steady flamelet model to simulate two turbulent nonpremixed jet flames with fuels of hydrogen and of methane. Statistics agreed between ISAM and the conventional approach, verifying the ISAM implementation. The baseline cost of ISAM was shown to be comparable to that of previous pretabulation approaches after only 100–1000 timesteps for both hydrogen and methane chemical mechanisms, demonstrating the minimal overhead incurred by traversing binary trees and the insensitivity of the cost to the size of the chemical mechanism. Though the test configurations simulated in this work are relatively simple nonpremixed flames, ISAM has the potential to enable a new generation of more complex manifold-based models that are far more generally applicable to multi-modal, non-adiabatic, or non-isobaric combustion, or combustion featuring multiple and/or inhomogeneous inlets with more complex subfilter PDFs.

Declaration of Competing Interest

None.

Acknowledgments

The authors gratefully acknowledge funding from the Army Research Office (ARO) Young Investigator Program (YIP) under grant W911NF-17-1-0391 and the National Aeronautics and Space Administration (NASA) under grant NNX16AP90A. C.E.L. gratefully acknowledges the Daniel and Florence Guggenheim Foundation Fellowship for additional funding support. The simulations presented in this article were performed on computational resources supported by the Princeton Institute for Computational Science and Engineering (PICSciE) and the Office of Information Technology's High Performance Computing Center and Visualization Laboratory at Princeton University.

References

[1] S. Pope, *Prog. Energy Combust. Sci.* 11 (2) (1985) 119–192.
[2] P.A. McMurthy, S. Menon, A.R. Kerstein, *Proc. Combust. Inst.* 24 (1) (1992) 271–278.
[3] P.-D. Nguyen, L. Vervisch, V. Subramanian, P. Domingo, *Combust. Flame* 157 (1) (2010).
[4] M.E. Mueller, *Combust. Flame* 214 (2020) 287–305.
[5] J. Oijenvan, F. Lammers, L. Goey, de, *Combust. Flame* 127 (3) (2001) 2124–2134.
[6] B. Marracino, D. Lentini, *Combust. Sci. Technol.* 128 (1–6) (1997) 23–48.
[7] C. Bekdemir, L.M.T. Somers, L. Goeyde, *Proc. Combust. Inst.* 33 (2) (2011) 2887–2894.
[8] M. Ihme, Y.C. See, *Proc. Combust. Inst.* 33 (1) (2011) 1309–1317.
[9] L. Gomet, V. Robin, A. Mura, *Combust. Flame* 162 (3) (2015) 668–687.
[10] B.A. Perry, M.E. Mueller, A.R. Masri, *Proc. Combust. Inst.* 36 (2) (2017) 1767–1775.
[11] M.E. Mueller, H. Pitsch, *Combust. Flame* 159 (6) (2012) 2166–2180.
[12] S. Weise, C. Hasse, *Parallel Comput.* 49 (C) (2015) 50–65.
[13] K.A. Kemenov, S.B. Pope, *Combust. Flame* 158 (2) (2011) 240–254.
[14] L. Shunn, *Large-eddy Simulation of Combustion Systems with Convective Heat-Loss*, 2009.

[15] S.B. Pope, *Combust. Theor. Model.* 1 (1) (1997) 41–63.
[16] H. Pitsch, N. Peters, *Combust. Flame* 114 (1) (1998) 26–40.
[17] R.S. Barlow, J.H. Frank, A.N. Karpetis, J.-Y. Chen, *Combust. Flame* 143 (4) (2005) 433–449.
[18] N. Peters, *Prog. Energy Combust. Sci.* 10 (3) (1984) 319–339.
[19] N. Peters, *Combust. Sci. Technol.* 30 (1–6) (1983) 1–17.
[20] A.W. Cook, J.J. Riley, *Phys. Fluids* 6 (8) (1994) 2868–2870.
[21] C.D. Pierce, P. Moin, *Phys. Fluids* 10 (12) (1998) 3041–3044.
[22] B.A. Perry, M.E. Mueller, *Proc. Combust. Inst.* 37 (2) (2019) 2287–2295.
[23] G. Lodier, L. Vervisch, V. Moureau, P. Domingo, *Combust. Flame* 158 (10) (2011) 2009–2016.
[24] O. Desjardins, G. Blanquart, G. Balarac, H. Pitsch, *J. Comput. Phys.* 227 (15) (2008) 7125–7159.
[25] J.F. MacArt, M.E. Mueller, *J. Comput. Phys.* 326 (2016) 569–595.
[26] M. Germano, U. Piomelli, P. Moin, W.H. Cabot, *Phys. Fluids A – Fluid.* 3 (7) (1991) 1760–1765.
[27] M.E. Mueller, PDRs, https://ctrfl.princeton.edu/software/.
[28] R.S. Barlow, Sandia H2/He Flame Data - Release 2.0, 2003, http://www.ca.sandia.gov/TNF.
[29] R.S. Barlow, C.D. Carter, *Combust. Flame* 97 (3) (1994) 261–280.
[30] R.S. Barlow, C.D. Carter, *Combust. Flame* 104 (3) (1996) 288–299.
[31] S.G. Davis, A.V. Joshi, H. Wang, F. Egolfopoulos, *Proc. Combust. Inst.* 30 (1) (2005) 1283–1292.
[32] R.S. Barlow, J.H. Frank, *Proc. Combust. Inst.* 27 (1) (1998) 1087–1095.
[33] G.P. Smith, D.M. Golden, M. Frenklach, GRI-Mech 3.0. http://www.me.berkeley.edu/gri_mech/.
[34] H. Pitsch, *Proc. Combust. Inst.* 29 (2) (2002) 1971–1978.
[35] W. Han, V. Raman, M.E. Mueller, Z. Chen, *Proc. Combust. Inst.* 37 (1) (2019) 985–992.